The Journal of the Astronautical Sciences, Vol. 57, No. 3, July–September 2009, pp. 667–688

Flux-Pinned Interfaces for the Assembly, Manipulation, and Reconfiguration of Modular Space Systems[1]

Joseph P. Shoer[2] and Mason A. Peck[3]

Abstract

Non-contacting interactions between permanent magnets and superconductors known as "flux pinning" provide a novel way to fix many modular space systems in desired relative positions and orientations, from space stations to close-proximity formations. When cooled appropriately, these flux-pinned interfaces require no power or active control and very little mass but provide very high mechanical stiffness (>200 N/m for a few hundred grams of material) and damping (2% of critical) between modules, making the technology ideal for in-orbit assembly applications. We describe new measurements and simulations to characterize these values for spacecraft applications. Flux-pinned interfaces have so far achieved inter-module separations in the 8–10 cm range with ~100 g of mass on each module, with the prospect of larger separations. We also discuss several means to actuate the noncontacting couplers, which is a first step toward the development of devices for the noncontacting manipulation and reconfiguration of modular space systems.

Introduction

New approaches to the assembly of modular structures in space will be important for future space-system architectures. The challenges of constructing the International Space Station and any potential successor systems, performing rendezvous of disparate elements of a multivehicle mission, dispatching self-repairing or adaptable probes to other bodies in the solar system, and maintaining complex formations in orbit require other paradigms than the adaptation of terrestrial construction techniques to on-orbit assembly of large structures. In this spirit, we

[1]Presented at the AIAA Guidance, Navigation, and Control Conference and Exhibit in Honolulu, HI, Aug. 18–21, 2008 as paper number AIAA-2008-7233. Approved for public release, distribution unlimited.
[2]Graduate Research Assistant, Department of Mechanical and Aerospace Engineering, 127 Upson Hall, Cornell University, Ithaca, NY 14853.
[3]Assistant Professor, Department of Mechanical and Aerospace Engineering, 212 Upson Hall, Cornell University, Ithaca, NY 14853.

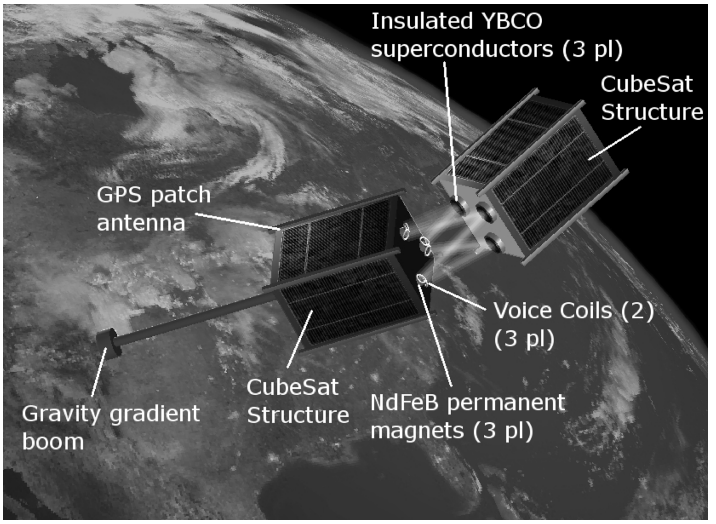

FIG. 1. A Non-Contacting, Modular CubeSat Spacecraft Concept with a Flux-Pinned Interface Capable of Action-at-a-Distance 6DOF Actuation.

have proposed a novel architecture wherein modular space assemblies lock themselves together with noncontacting interactions provided by an effect known as magnetic flux pinning [1]. In the present study, we further develop metrics for this concept with measurements of a flux-pinning interface for potential use in passively connecting spacecraft structures without mechanical contact. These metrics include the stiffness of flux-pinned interfaces under dynamic conditions, correlation of experiments to simplified numerical models, and determination of the design space of such interfaces in terms of mass.

These space systems blur the distinction between mechanically linked modular structures and formation-flying clusters of spacecraft. They span a wide range of scales, from picosatellite clusters to space stations. A noncontacting architecture based on action-at-a-distance forces confers several advantages over traditional space-assembly paradigms. The safety and robustness of the assembly process would be greatly enhanced, because the integration of a new module onto a structure may only involve maneuvering it within pinning range and then activating the noncontacting interfaces. The need for hazardous spacewalks or complex robotic operations to assemble large structures would be mitigated. These modular systems use interactions that ensure modules never touch one another, eliminating collision risks, while still maintaining basins of attraction that enable passive assembly processes.

Figure 1 shows a simple, CubeSat-based fractionated spacecraft assembled from such noncontacting modules. Each module is structurally identical, simplifying integration, test, and operations. Depending on the design of the interface, this system may be assembled in any one of several different physical configurations and might even be capable of reconfiguring itself. The assembled spacecraft can change its inertia properties, realize new functionality, or restore damaged components through these reconfigurations. As a more specific example, stationkeeping and reconfiguration of sparse-aperture telescope formations are ideal applications of this type of noncontacting architecture, which allows both passive and active control of the modular components [2, 3]. Another tantalizing possibility

is that many small flux-pinned modules may form a solar sail with structure provided by massless magnetic fields [4].

At the core of this paradigm is magnetic flux pinning, an interaction between type II high-temperature superconductors (HTSC) and magnetic fields. On a fundamental level, flux pinning is a quantum effect, but it has macroscopic effects that are easy to observe. All superconductors completely repel weak magnetic fields because the fields excite supercurrent loops within the zero-resistance HTSC. The magnetic field generated by these supercurrents exactly opposes the applied field, causing the net field within the HTSC material to be zero; this repulsion is known as the Meissner effect [5]. However, type II HTSCs, such as yttrium barium copper oxide (YBCO), are laced with impurities that form sites where sufficiently strong magnetic fields, with flux density above a HTSC-specific critical value [7], penetrate the superconducting material. The applied magnetic field lines become trapped on these impurities in the HTSC. Supercurrents excited by the applied field oppose any motion of the flux lines away from such "pinning" sites [5].

The most readily observed macroscopic behavior is the levitation of a permanent magnet over a HTSC. After the field lines of the magnet are pinned, the superconductor effectively resists any change in the magnetic flux distribution within its volume. This resistance comes from shifts in the distribution of supercurrents within the HTSC, and it manifests itself as a force and torque on the magnet. The magnet is subject to a nonlinear, hysteretic restoring force pushing it toward a six-dimensional equilibrium and strong damping force similar to eddy-current damping. A simple (and effective, for small motions) model of a flux-pinned magnet–superconductor pair connects the two bodies by a multiple-degree-of-freedom (DOF) spring and damper [6, 7].

Two features of flux pinning make it attractive for space applications. First, it is an action-at-a-distance force but is not subject to the limitations described by Earnshaw's Theorem. A consequence of this theorem is that a configuration of force sources that obey an inverse-square law (e.g., gravitational, electrostatic, or magnetostatic force) cannot be passively stable [8]. Flux pinning, instead, can create passively stable 6DOF equilibria among multiple bodies in space because the magnetic field of the supercurrents depends on the motions of flux-pinned magnets. Second, this effect does not require power if the superconductor is passively cooled. As long as the HTSC material remains in its superconducting state (that is, below its critical temperature: $T_c \approx 88$ K for YBCO), it pins magnetic flux. HTSCs may require power for cooling if they receive incident sunlight, however, depending on the characteristics of the local environment, passive cooling may be sufficient: for example, the equilibrium temperature of the Spitzer Space Telescope is near 30 K, sufficiently low for flux pinning [9]. No voltage need be applied to the superconductor, and no actuation of the magnet is required. The power and fuel savings for formation flight missions are potentially significant, and substantial mass savings might be realized for certain applications and capabilities by using flux-pinned interfaces instead of conventional docking hardware or conventional attitude-control systems on modular or formation-flying missions. Furthermore, the prospect of passive stability following any of several power- or propulsion-related failures is an attractive possibility for any spacecraft for which fault tolerance is expected. Data and software-related failures would not result in instability. The force exerted by flux pinning can be highly hysteretic with some HTSCs. This feature has two important implications for the application of

flux pinning to spacecraft station-keeping and modular assembly. First, constant-parameter linear models of flux-pinning force as a spring and damper are accurate only for small relative motions between the magnet and superconductor. For a system in or near equilibrium, this assumption is reasonable. Second, there is no single equilibrium for a specific magnet-superconductor pair. Rather, many different equilibria are possible, depending on the history of the system (for instance, whether the superconductor was cooled with the magnet already at its desired equilibrium, or whether the magnet moved in from infinity after cooling) [5]. The versatility of such an interface to establish a wide range of equilibria also extends to HTSCs that exhibit little or no hysteresis. We view these subtleties as effects that can be exploited rather than problems to be overcome.

In previous work, we established that flux pinning provides stiffness sufficient to maintain the structure of modular space systems with an intermodule spacing up to approximately 5–7 cm for magnets and superconductors of modest mass (~30 g). We investigated the stiffness of a flux-pinned magnet-superconductor pair over a variety of equilibrium separations and found sufficient stiffness for close-proximity spacecraft formation or docking maneuver applications, as high as 250 N/m for spacing less than 1 cm. These experiments characterized flux-pinning in quasistatic situations, in which we determined stiffness from the relation between the force exerted by flux pinning as the magnet underwent small displacements relative to the superconductor [1]. Others have examined the properties of magnetic flux pinning from the perspective of levitation in 1 *g* [5, 10–12]. Flux-pinning force exerted in the direction perpendicular to a superconductor's surface has therefore been well characterized. The applications we have in mind take advantage of the fact that flux pinning affects the other rigid-body DOF as well. These applications also demand that some attention be paid to the dynamics, in addition to the static loads.

This article describes a new system-identification experiment with the objective of developing metrics to characterize the stiffness and damping of flux-pinned interfaces for spacecraft applications, and proposes means to precisely manipulate the interfaces with action-at-a-distance forces. The next section explores the physical properties of a flux-pinned interface, with relevant applications to space systems described throughout. The article then discusses models of the flux-pinning effect to correlate the experimental data and simulate new space systems. The following sections describe our experiment and results, corroborated with the model. An approach to reconfigurable spacecraft based on flux pinning may lead to additional exciting applications. These investigations may enable the development of a reconfigurable, modular space system that is capable of assembling passively, integrating new components after its initial deployment, adapting itself to new mission roles, and repairing damaged systems autonomously.

Properties of the Interface

Prior investigations, both experimental and theoretical, have determined some of the basic properties of the stiffness and damping of a magnet flux-pinned to a superconductor [6, 7, 13]. Although the force between a permanent magnet and HTSC is, in general, hysteretic, small relative displacements yield force-versus-displacement curves that follow repeatable minor loops. This property allows the interaction to be modeled as a linear restoring force with a linear stiffness constant for small motions. Flux-pinning damping similarly resembles linear viscous damp-

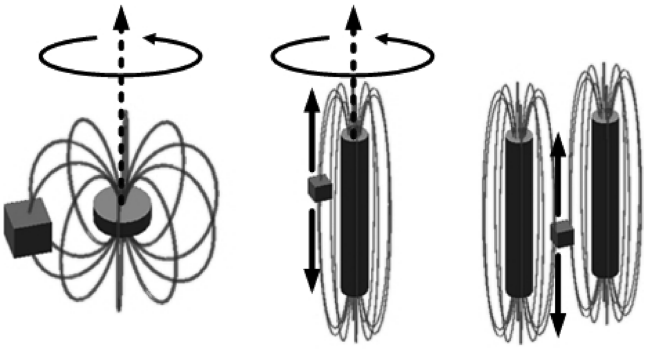

FIG. 2. Kinematic mechanisms formed by flux pinning a superconducting cube to the fields of permanent magnets. The cube may freely undergo only the indicated motions. *Left to right*: revolute joint, cylindrical joint, and prismatic joint.

ing for small motions. These linear properties hold regardless of the thermal and magnetic history of the interface. "Field cooling" occurs when the HTSC cools below its critical temperature with a magnet in pinning range, penetrating the HTSC with its field. "Zero-field cooling" is the case where a HTSC cools in the absence of any field and the magnet subsequently approaches from infinity, experiencing a hysteretic force before undergoing its small displacements [13]. However, the stiffness and damping forces acting on the flux-pinned pair are quantitatively different in the zero-field cooled and field-cooled cases [13]. The investigations in this work take place in field cooling, because this scenario would be the likely case if modules in space activate and deactivate their flux-pinned interfaces by altering the temperature of the HTSCs. Field cooling also provides a stable interaction in cases where hysteresis is not present [13].

The stiffness and damping of flux-pinned interfaces (FPI) obey certain quantitative relationships. Previous work has established that the translational stiffness between a magnet and field-cooled HTSC drops exponentially with distance as the initial pinning separation increases [14]. In 2007, we confirmed this property for translational stiffness in both the direction perpendicular to the HTSC surface and a direction in the plane of the surface [1]. The lateral and perpendicular stiffnesses also obey the particular relationship that stiffness for small motions perpendicular to the HTSC surface is generally twice that for small motions along the surface. Others have measured this property experimentally and have proved it theoretically [13, 15] and we confirmed it in [1].

A flux-pinned interface also has the ability to pin only select degrees of freedom. Figure 2 shows three basic joints that can be assembled from permanent magnets and a HTSC by taking advantage of this principle [16]. Because flux pinning does not constrain motions that preserve the magnetic field distribution inside the superconducting volume, designing a flux-pinned joint is equivalent to designing a magnetic field that remains constant under motions along the desired degree(s) of freedom. The simplest joint formed by a magnet–HTSC pair is a revolute joint (Fig. 2, left), in which the HTSC is free to spin about the magnet's dipole axis, remaining at constant radius from the dipole center. An elongated, cylindrical magnet has a nearly uniform vertical field close to its midpoint, allowing a cylindrical joint in which the HTSC slides along the magnet's axis over a limited range (middle). Finally, an additional permanent magnet constrains

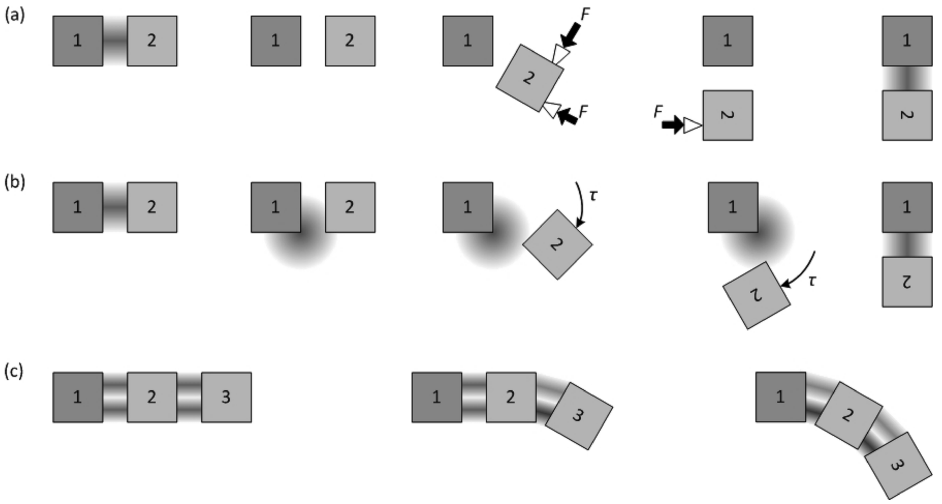

FIG. 3. Three possible modes of reconfiguration. (*a*) Flux pinning fixes modules only in their initial and end states, other actuators (such as the thrusters shown) are used for the reconfiguration. (*b*) Flux pinning selects the available degrees of freedom between modules; in this example they hinge. (*c*) Electromagnets bend flux-pinned interfaces and articulate a modular structure.

rotations of the HTSC, creating a prismatic joint (right). The high field gradients near the ends of each magnet act as noncontacting limit stops, preventing the HTSC from moving beyond a certain range.

There are several means by which FPIs consisting of HTSCs and magnets enable modular space systems capable of reconfiguration. Figure 3 is a schematic of three of the many possible sequences of reconfiguration for simple modular systems, each with different results. These sequences rely on three properties of FPIs. First, FPIs are "switchable"; that is, the existence of flux-pinning forces depends on the thermal state of the superconductor in a binary fashion. Second, a magnetic field source feels no flux-pinning force or torque about any axis of symmetry in its field. For example, the axisymmetric field of a dipole is free to spin about its axis when flux-pinned. Third, other noncontacting forces can perturb an established flux-pinning equilibrium.

Sequence (a) in Fig. 3 demonstrates reconfiguration via the switchability property of FPIs. The FPI connecting two pinned modules might be deactivated by warming its superconducting elements above T_c, freeing the modules to move. In space, the HTSCs can be warmed simply by exposing them, or a spacecraft–bus face on which they are mounted, to sunlight. Traditional attitude-control actuators such as reaction wheels and thrusters might then be used to reposition the modules. Once components achieve a desired set of positions and orientations, the FPI can be reactivated (by shielding the HTSC from sunlight) to impose restoring and damping forces between the modules, locking them into a new configuration. The major disadvantage of this sequence is that it separates system components and is subject to the complexities of close-proximity formation flight and docking maneuvers, eliminating several advantages conferred by the flux-pinned interfaces during the reconfiguration process.

In sequence (b), the interface includes arrays of electromagnets oriented such that the deactivation of some magnets gives a net field with cylindrical symmetry.

This symmetry creates a hinge from the pinning interface. Rotations about the symmetry axis of the field produce no torque, while other DOF (translation and rocking rotations with respect to the superconductor) remain stiffened by the restoring force and torque of flux pinning [5]. The spacecraft modules now form a noncontacting mechanism that allows them to morph into a new configuration before the electromagnets are reactivated, stiffening motion in the remaining DOF and fixing the modules in place once again. At no point does the FPI disconnect; the modules always remain near each other and rotate around only the defined axis of symmetry. This basic hinge concept can be used to build modular systems that reconfigure by forming an appropriate kinematic mechanism [16]. Wilson, Shoer, and Peck describe an experimental implementation of the maneuver depicted in Fig. 3(b) [17]. A space structure of flux-pinned modules, such as the concept in Fig. 1, can perform reconfiguration maneuvers by selecting appropriate joints at each interface to provide the required kinematic degrees of freedom.

Finally, the bottom sequence in Fig. 3 takes advantage of the continuum of equilibria afforded by flux pinning. This continuum gives an FPI some degree of malleability: pinned modules bend into a new configuration via distortion of the magnetic field. An FPI might achieve this new configuration by actuating the current in pinned electromagnets, activating secondary electromagnets arrayed around a pinned permanent magnet, or moving a ferromagnetic material near the superconductors. Depending on how the actuation is applied and the hysteretic properties of the superconductors, this deformation of a modular formation might be permanent or might relax when the actuation ceases. The FPIs retain their switchability features. So, a modular structure might form itself into an arm like that in Sequence (c) as one means to achieve pick-and-place reconfiguration as in Sequence (a).

There are several ways to actuate an active FPI. For instance, nearby materials with magnetic properties have a perturbation effect on the interface. Such elements include ferromagnetic materials near the superconductor, which distort the pinned field and change the behavior of the interaction. Perturbations can also come from electromagnets positioned near the HTSC, which activate after the permanent magnet has been pinned and force more flux into the HTSC, altering how the superconductor responds to motions of the pinned magnet. As another example, an active electromagnet flux pinned to a HTSC can be tuned after pinning is established to change the properties of the FPI. Behavior changes are possible through modification of the equilibrium separation between the HTSC and flux-pinned magnet and through modification of the stiffness or damping forces experienced by the pinned magnet–superconductor pair.

Image-Dipole Model

In some cases, an effective representation of the magnetic field of the HTSC is the field produced by two virtual *image magnets* within the superconductor. This *frozen-image model* mimics the effect of the superconductor on the external magnetic field, giving analytical expressions for simulation [18]. This model applies when the superconductor is field-cooled, the magnet–superconductor separation is much greater than the superconductor's skin depth, and hysteresis is negligible. These conditions are consistent with the experiments reported here: we field-cool the superconductors; the magnet–superconductor separation d is greater than the total depth of the superconducting disc; and hysteresis is low. The field of a dipole is a reasonable approximation for a permanent magnet as long as any test

point in this field is far from the magnet edge. At position $\mathbf{r}$ and with dipole moment vector $\mathbf{n}$, the field is

$$\mathbf{B} = \frac{\mu_0}{4\pi r^3}(3(\mathbf{n} \cdot \hat{\mathbf{r}})\hat{\mathbf{r}} - \mathbf{n}) \tag{1}$$

where the hat denotes a unit vector. This field interacts with two images within the superconductor. One, the frozen image, appears at a position vector reflected across the superconductor surface from the external magnet's position. The field from the frozen image develops when the superconductor is first field-cooled, and the image remains at this position and orientation as long as the superconductor remains below its critical temperature. Its dipole vector is identical to that of the external magnet at the instant of field cooling. Therefore, the frozen image attracts the external magnet for small relative displacements and rotations. If the superconductor surface passes through the origin and has normal vector $\hat{\mathbf{a}}$, then the reflection of a vector $\mathbf{r}$ across this plane is

$$\mathbf{r}_{\text{reflected}} = \mathbf{r} - 2(\hat{\mathbf{a}} \cdot \mathbf{r})\hat{\mathbf{a}} \tag{2}$$

Thus, the field of the frozen image is

$$\mathbf{B}_f = \frac{\mu_0}{4\pi\|\boldsymbol{\rho}_f^3\|}(3[(2(\hat{\mathbf{a}} \cdot \mathbf{n}_{\text{FC}})\hat{\mathbf{a}} - \mathbf{n}_{\text{FC}}) \cdot \hat{\boldsymbol{\rho}}_f]\hat{\boldsymbol{\rho}}_f - (2(\hat{\mathbf{a}} \cdot \mathbf{n}_{\text{FC}})\hat{\mathbf{a}} - \mathbf{n}_{\text{FC}})) \tag{3}$$

where $\boldsymbol{\rho}_f = \mathbf{r} - \mathbf{r}_{\text{frozen}} = \mathbf{r} - \mathbf{r}_{\text{FC}} + 2(\hat{\mathbf{a}} \cdot \mathbf{r}_{\text{FC}})\hat{\mathbf{a}}$ represents the relative position and subscript FC represents the position and orientation vectors at the time of field-cooling. The position vector $\mathbf{r}$ of the flux-pinned dipole may vary with time.

The other image is a mobile image that moves with the external magnet. At any time, it appears at the reflected position vector of the external magnet with a dipole axis vector also reflected from that of the external magnet. The mobile image, which mimics Meissner-effect exclusion of magnetic fields from the superconductor, generally repels the external magnet. The field of the mobile image resembles that of the frozen image

$$\mathbf{B}_m = \frac{\mu_0}{4\pi\|\boldsymbol{\rho}_m^3\|}(3[(\mathbf{n} - 2(\hat{\mathbf{a}} \cdot \mathbf{n})\hat{\mathbf{a}}) \cdot \hat{\boldsymbol{\rho}}_m]\hat{\boldsymbol{\rho}}_m - (\mathbf{n} - 2(\hat{\mathbf{a}} \cdot \mathbf{n})\hat{\mathbf{a}})) \tag{4}$$

A key difference in the equations for the field of the frozen and mobile images is that the quantities that determine the mobile image field, including the relative position $\boldsymbol{\rho}_m = \mathbf{r} - \mathbf{r}_{\text{mobile}} = 2(\hat{\mathbf{a}} \cdot \mathbf{r})\hat{\mathbf{a}}$, may vary with time. Once the frozen and mobile image fields are known, the force and torque on the external dipole with axis $\mathbf{n}$ are straightforward to calculate

$$\mathbf{F} = \nabla(\mathbf{n} \cdot (\mathbf{B}_f + \mathbf{B}_m)) \qquad \boldsymbol{\tau} = \mathbf{n} \times (\mathbf{B}_f + \mathbf{B}_m) \tag{5}$$

Stiffnesses can be calculated either numerically or by evaluating partial derivatives of the force and torque given by these expressions. However, damping ratios for the flux-pinned magnet and superconductor cannot be calculated from this model because the damping arises from hysteretic losses, which are not described by the image magnets.

One great advantage of the frozen-image model is that it does not require the extensive numerical computations of, for instance, simulating supercurrent distribu-

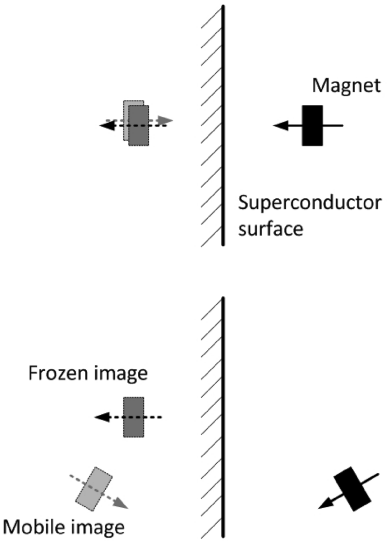

FIG. 4. Image-dipole model of flux pinning. *Top*: frozen and mobile images appear within the superconducting volume upon field-cooling. *Bottom*: the frozen image remains fixed, while the mobile image moves with the magnet.

tions. The model provides design intuition for the magnet–superconductor interaction. Several features of the interaction are evident in Fig. 4. The field-cooled position of the magnet is the interface equilibrium because the two image dipoles coincide when the magnet is in this position, giving a net zero field and therefore no force. Furthermore, this equilibrium is stable, because the frozen image attracts the magnet toward it while the mobile image always repels it: if the magnet moves closer to the HTSC surface, the repelling image is closer and thus exerts a greater force on the magnet. The reverse is true when the magnet displaces away from the superconductor. Similar relations for magnet displacements along the superconductor surface demonstrate stability in that direction as well. In addition, the nonlinearity of the system is apparent from the varying separations between the magnet and its images and the fact that magnetic fields fall off with the inverse cube of distance. Finally, the image model offers insight into why Earnshaw's Theorem does not limit flux pinning: the motions of the mobile image have a direct parallel to active control, which can maintain stable equilibria between magnets.

This model reproduces and extends our 2007 results. It provides a basis for calculating the six-dimensional stiffness matrix for an arbitrary collection of magnets and superconductors, provided that the collection is consistent with the assumptions of the image model. Because there are simple analytical expressions for dipole fields, we can easily simulate the fields numerically if the magnets involved are very close to dipoles. Figure 5 mimics in simulation a plot showing data obtained experimentally in 2007 (Fig. 12 in reference [1]). These numerical results confirm that the flux-pinned stiffness of a paired magnet and superconductor has a power-law dependence on the flux density projected to the superconductor surface.

The frozen image represents the magnetic flux distribution from supercurrents excited by the flux-pinned magnet, but the frozen image persists even if the field-cooled magnet moves far away from the superconductor. This persistent image interacts with any other magnet that approaches the superconductor surface as long as

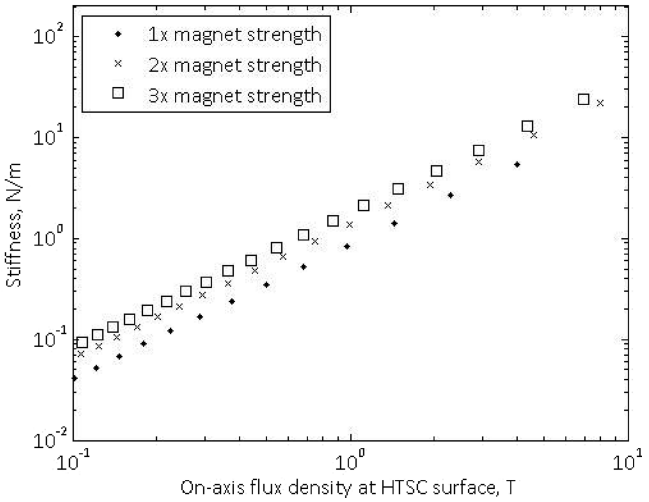

FIG. 5. Log-Log Plot of Translational Stiffness of a Flux-Pinned Magnet-Superconductor Pair Against Flux Density at the Superconductor Surface.

the superconductor temperature remains below T_c. This property suggests that a superconductor can be "preloaded" with a magnetic flux distribution so that magnets are passively attracted to the established noncontacting 6DOF equilibrium. In this way, flux-pinned interfaces enable passive self-assembly of modular spacecraft that never have come into contact with one another before assembly begins.

Experiment

The experimental apparatus is designed to characterize the 6DOF stiffness and damping of a FPI under a variety of conditions using system-identification techniques. Similar experiments have been performed in the context of superconducting levitation applications, where a magnet is levitated over an HTSC and then its position measured as it vibrates in response to some input [13, 19]. However, because we envision flux pinning applications in zero gravity, experiments reported here are not restricted to levitation. Levitation involves an equilibrium between flux pinning and gravitational forces, whereas the objectives of these experiments include characterizing only flux pinning.

Figure 6 is a schematic of the experimental setup. A field-cooled single-domain YBCO disc with diameter 56 mm and height 20 mm is immersed in a liquid nitrogen bath with its axis of symmetry oriented horizontally, i.e., along the experiment's x axis. A translation stage precisely positions the superconductor near a permanent magnet. The stage allows magnet–superconductor separations from $d = 5$ cm to about 1.5 m. The magnet itself is the bob of a $\sim$3.5 m long pendulum The pendulum constrains motions of the magnet in the direction of gravity and severely limits rotations of the magnet about its dipole axis but allows motion in all other rigid-body DOF. The constrained motions are either equivalent to other motions by symmetry or are unaffected by flux pinning. The pendulum dynamics affect the four remaining modes in a quantifiable manner.

The inputs and outputs chosen for system identification do not interfere with the motion of the magnet relative to the superconductor. A simple coil of wire supplied with a computer-controlled current drives the flux-pinned system. This electromagnet

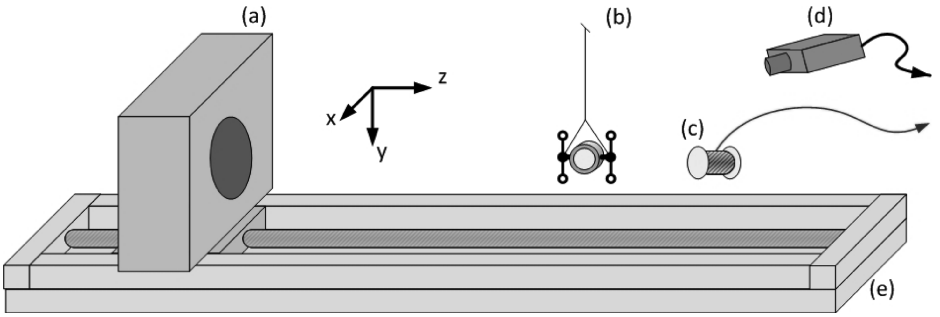

FIG. 6. Experimental setup, showing the placement of the (*a*) vertically-mounted YBCO superconductor in its liquid nitrogen bath, (*b*) pendulum with permanent magnet and tracking flags, (*c*) input coil, (*d*) motion-capture camera system, and (*e*) translation stage.

does not contain a ferromagnetic core, which keeps it from offsetting the flux-pinned magnet's equilibrium. A motion-capture camera system tracks the resulting movements of the pendulum bob with a minimum frame rate of 105 fps, allowing frequency measurements up to at least 10 Hz. Reducing the region of interest of the camera detector allows it to achieve higher frame rates and reliably measure frequencies up to 15 Hz. Low-mass flags with target-tracking points on the pendulum bob and a contrasting black background behind the pendulum facilitate motion capture.

The motion-capture data describe the position of the tracking flags in the camera's field of view. The actuating electromagnet coil and motion-capture camera excite and measure each of the fundamental modes of the pendulum bob. The modes of the unpinned pendulum include swinging motion in the directions parallel (x) and perpendicular (z) to the superconductor surface, twisting rotation about the monofilament axis, and rocking rotations about the axis perpendicular to both the magnetic dipole axis and pendulum axis. Rolling motion of the magnet is not affected by flux pinning because this motion is a rotation about the magnetic dipole axis. It is limited by the construction of the pendulum bob and enters into the system only as a higher-order pendulum mode. Figure 7 shows these mode shapes. Fast Fourier transforms (FFTs) of position time histories from the tracking camera provide the spectral content of the pendulum motion. A set of second-order system models fit to the FFTs model stiffness and damping for the flux-pinned interface.

The resonant frequencies in each FFT decompose into a combination of the free pendulum frequency and frequency introduced by flux-pinning stiffness. The one-dimensional equation of motion for a pendulum bob connected to a vertical wall by a spring is

$$\ddot{z} = -\frac{k}{m}z - \frac{g}{l}z = -\left(\frac{k}{m} + \frac{g}{l}\right)z \tag{6}$$

for small motions of the pendulum bob. The frequency of oscillation for the composite system, therefore, is

$$\omega = \sqrt{\frac{k}{m} + \frac{g}{l}} = \sqrt{\omega_{\text{pinning}}^2 + \omega_{\text{pendulum}}^2} \tag{7}$$

Thus, the resonance introduced by flux-pinning stiffness adds in root-sum-square fashion to the existing pendulum frequency. Frequencies related to other stiff

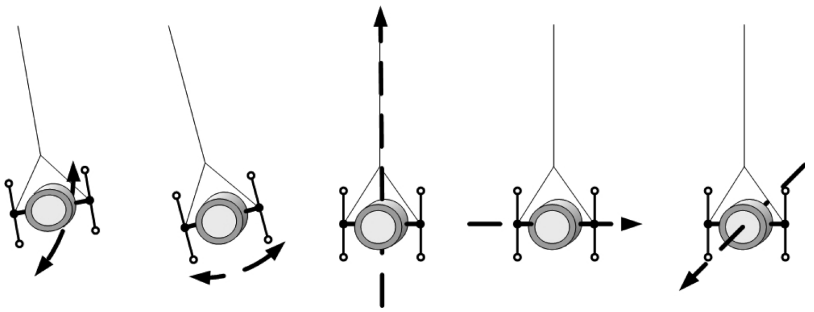

FIG. 7. Modes of the pendulum bob. From left to right: swinging (perpendicular to the high-temp superconductor (HTSC)), swinging (parallel to the HTSC), twisting, rocking, and rolling motion. Note that there are two swinging modes, oriented to the superconductor surface (x and z).

elements in the pendulum system (such as torsion of the pendulum bob about the pendulum axis) similarly combine in this fashion with flux-pinning frequencies. The frequency of each mode is unique due to the mass properties of the pendulum bob, with the exception of the two swing modes. These two modes are split by the unequal lateral and transverse flux-pinning stiffnesses. Thus, the frequencies of each distinct DOF can be identified in the FFTs.

The pendulum arrangement is versatile and can accommodate many experiments to determine the behavior of a flux-pinned interface under different perturbations. Experiments to characterize the dynamic stiffness and damping of flux pinning involve tracking pendulum motions when the actuating coil applies impulses, sine sweeps, Gaussian noise, or other inputs. Simple initial tests determine the range of distances over which flux pinning acts for various types of magnets and superconductors. More subtle tests include modifying the interface with other conductive materials in an effort to establish the feasibility of different ways of adjusting stiffness, damping, and equilibrium position.

Results and Discussion

Range of Flux Pinning

To establish a FPI between a magnet and superconductor, the magnet must project a minimum field into the superconducting volume. Any less than the minimum and the superconductor exhibits only Meissner repulsion of the magnet, which cannot establish a stable action-at-a-distance equilibrium. Measurements of the resonant frequencies of the pendulum as a function of magnet–superconductor separation clearly indicate the distance at which the magnet provides the minimum flux to the superconductor because the flux-pinning stiffness k_z is twice k_x. Therefore, the swing mode of the pendulum shifts from its unpinned frequency due to Meissner repulsion as it approaches the YBCO, but the resonance splits into two distinct modes when flux pinning is present.

Figure 8 shows a series of FFTs of the captured motion for varying magnet–superconductor separation distances, with one cylindrical NdFeB magnet approximately 3.8 cm in diameter and 1.3 cm tall on the pendulum and one single-domain YBCO disk. For distances ranging from approximately $d = 5$–7 cm, four resonance peaks appear in the Fourier spectrum (the detailed spectra show three of the four peaks). However, at $d = 8$ cm and beyond, two of the peaks have merged. The resonance splitting is qualitative evidence that the range of flux pinning for this magnet–

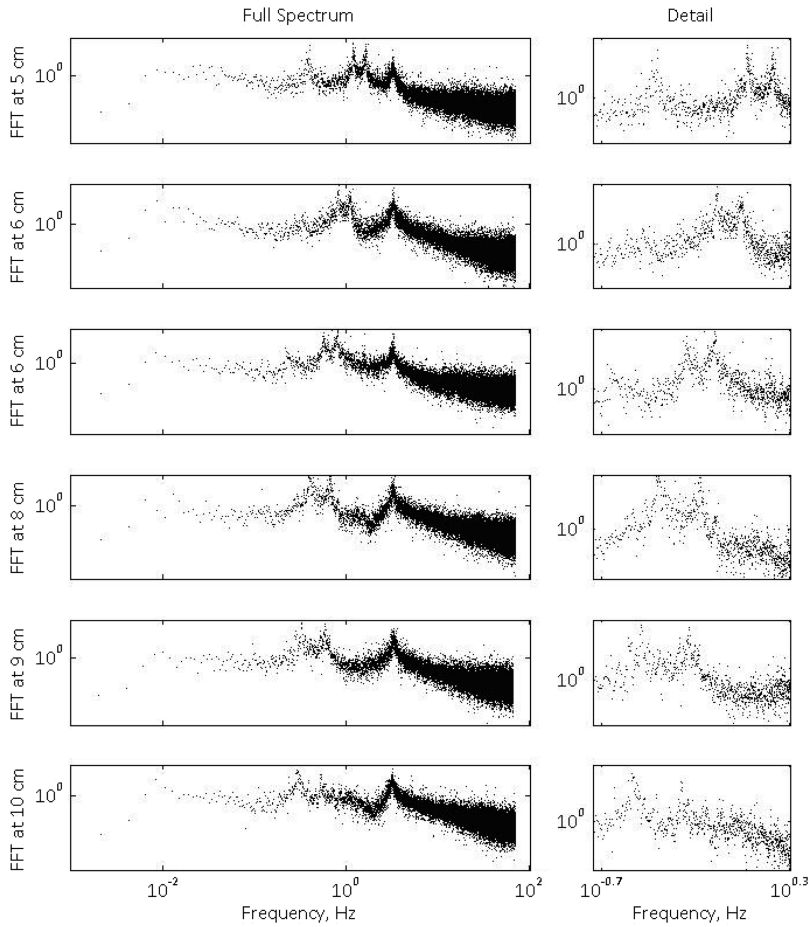

FIG. 8. Modification of Pendulum Modes, as Measured by Fast Fourier Transforms of Motion Capture Data.

superconductor configuration is approximately 7 cm. Other configurations, including larger single-domain YBCO discs and special arrangements of magnets, may increase this pinning range.

Pendulum Mode Modification

Fourier transform data such as that in Fig. 8 provide stiffness and damping data through fits of a simple harmonic oscillator model to each peak within its half-power bandwidth. The dependence of resonant frequency on separation is clear in Fig. 9, in which frequencies are plotted along with values obtained from the frozen-image model. Error bars on the plot show the SD in a pendulum frequency that was not modified by flux pinning. The values agree qualitatively, confirming that frequency decays exponentially with field-cooling separation until there is not enough flux penetrating the superconductor upon field cooling to allow flux pinning. At separations below this minimum-flux limit, about 9–10 cm in Figs. 9 and 10, flux pinning cannot affect the pendulum frequency. The frozen-image model of the pinned pendulum adopts the unmodified pendulum frequency beyond this separation distance to represent this effect. The decreasing trends of both the modeled and experimental data in Fig. 10 are consistent with the

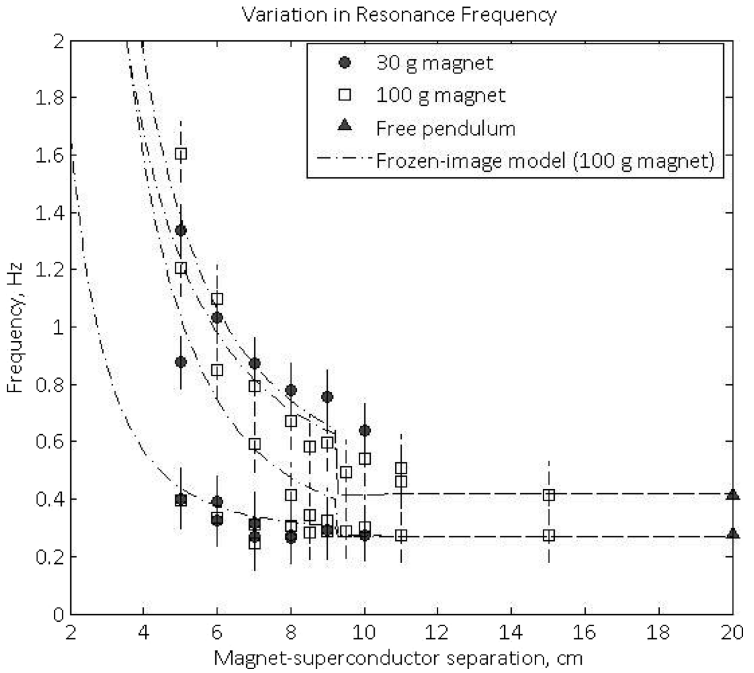

FIG. 9. Pendulum Frequency Modification as a Function of Field-Cooling Separation Distance, Data, and Frozen-Image Model.

conclusion from [1] that stiffness decays exponentially with pinning separation out to a limit at the maximum range of flux pinning. The image model correspondence with this data allows a better estimate of the maximum range of flux pinning than does that in the preceding section. We conclude that the 100 g NdFeB magnet and single-domain YBCO disc exhibit flux-pinning behavior at separations up to approximately 9–10 cm, with decreasing stiffness as the field-cooling separation increases.

Figure 10 shows the translational and rotational stiffnesses of two magnets flux-pinned to the YBCO discs as a function of field-cooling separation after the particular vibration modes from Fig. 9 were identified. Again, the frozen-image model matches the exponential decay trend of the plots for separation distances where flux pinning occurs. The upper points in the translational stiffness plot are associated with the pendulum swing mode in z. This value is a key performance parameter of a flux-pinned interface, because stiffness about other translational and rotational degrees of freedom can be constructed from k_z through various arrangements of axially stiff magnet–superconductor pairs. Figure 10 clearly indicates that a larger magnet enhances stiffness: the dipole moments of the 30 and 100 g rare-earth magnets are roughly proportional to their masses, and the 100 g magnet provides the FPI with a little over three times the stiffness k_z of the smaller 30 g magnet. In fact, the increased stiffness with a larger magnet corroborates the principle that the stiffness of a flux-pinned interface scales with the magnetic flux at the YBCO surface at the time of field-cooling according to a power law, as calculations with the frozen-image model show (in Fig. 5). The data in Fig. 11 support this experimentally for cylindrical magnets. We therefore regard the

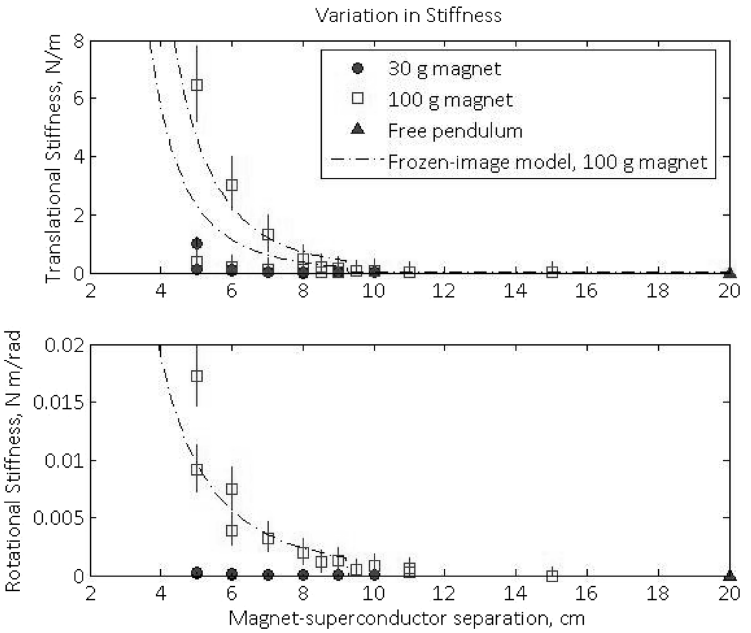

FIG. 10. Flux-Pinned Stiffness as a Function of Field-Cooling Separation Distance, Data, and Frozen-Image Model.

magnetic flux density projected onto the superconducting components of a flux-pinned interface as an important metric in optimizing the design of FPI hardware.

Figure 10 does not show the expected relationship of translational stiffnesses, that $k_z = 2k_x$ [13, 15]. The probable reason for this discrepancy is that the vibration mode shapes of the flux-pinned pendulum do not correspond directly to the Cartesian coordinates x and z. The normal modes of oscillation are, rather, swing along the superconductor surface normal and two combinations of the twist and swing modes. These modes of oscillation correspond to the "rolling" modes described in Sugiura et al. [11]. Frequencies and stiffnesses of these modes are shown here as "translation" or "rotation" according to the coordinate with which the mode shape is best aligned.

Damping in a flux-pinned magnet–superconductor pair results from hysteretic energy losses as the magnet moves relative to the superconductor. However, these data are unable to distinguish the damping ratio of the pendulum flux pinned to the single-domain YBCO from the damping naturally present in the pendulum. We conclude from the absence of damping that the single-domain superconductors exhibit very nonhysteretic interactions—a useful fact because it implies that hysteresis is low. This low damping validates one of the initial assumptions of the frozen-image model and allows us to neglect hysteresis in the treatment of similar flux-pinned interfaces based on these superconductors. Instead, the use of other materials, such as thin aluminum plates, can provide damping for a FPI through eddy-current effects, as described in the next section.

Performance Modification and Actuation of Flux-Pinned Interfaces

The properties and behaviors of a flux-pinned interface can be modified. Methods of doing so include adding passive hardware elements as perturbations on

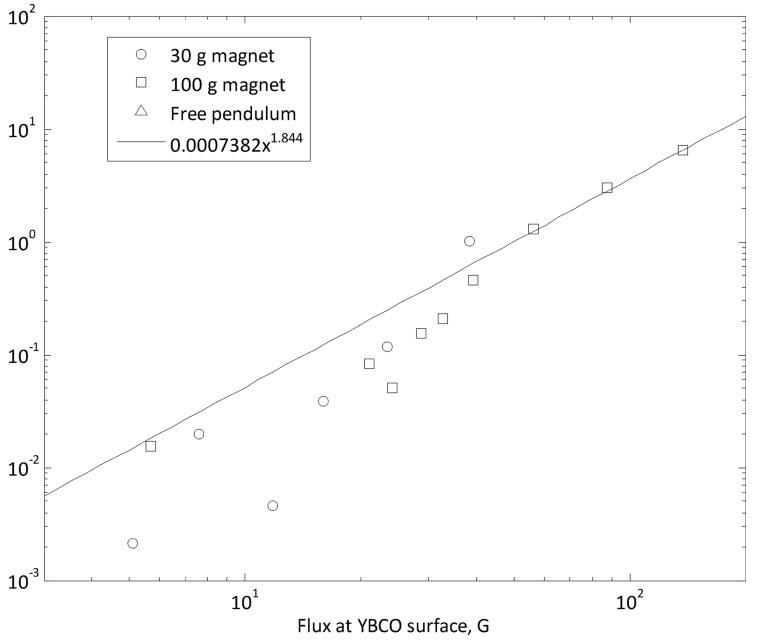

FIG. 11. Flux-Pinned Stiffness Versus Magnetic Flux Density at the Superconductor Surface Upon Field-Cooling.

the base FPI (such as ferromagnetic materials, diamagnetic materials, conductive metals, or permanent magnets) and flux pinning an electromagnet rather than a permanent magnet, and then actuating its field. This section examines the effect of these modifications on the equilibrium position of the pinned pendulum bob and the stiffness and damping of the flux-pinned interface through both frozen-image simulation and experiment.

Figure 12 illustrates how the presence of ferromagnetic material modifies the stiffness of the flux-pinned interface while maintaining the magnet–superconductor separation at its field-cooled value. In this experiment, the perturbation is an iron disc approximately the same size as the YBCO, placed on the opposite side of the superconductor from the magnet. Before field cooling, when the YBCO is not in

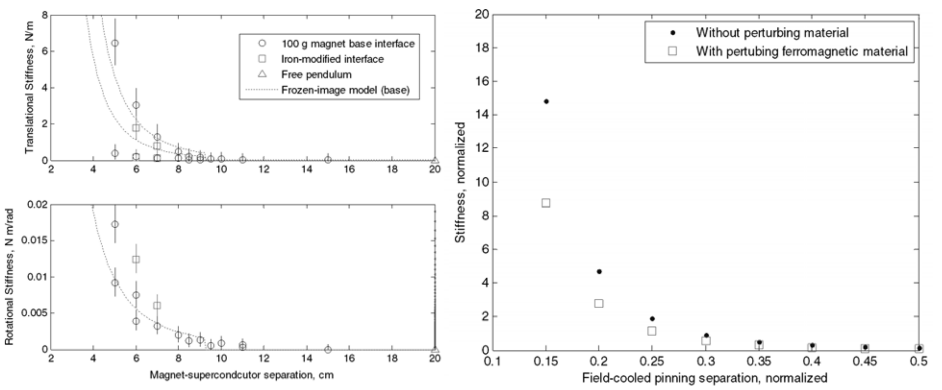

FIG. 12. Flux-pinned stiffness versus field-cooling separation in the presence of an iron plate. *Left:* experimental measurements, *right:* frozen-image model of k_z versus d with iron plate.

its superconducting state, the ferromagnetic disc attracts magnetic flux lines into the YBCO volume, changing the magnitude and gradient of the magnetic field within the superconductor. This configuration exhibits a number of qualitatively different effects. Translational stiffness k_z decreases, while k_x remains largely the same. Rotational stiffness (corresponding to the pendulum twist mode) increases. A simple simulation with the frozen-image model, treating the iron disc as another (weak) dipole attracting the flux-pinned magnet, also shows a drop in translational stiffness perpendicular to the superconductor. So, a design may trade one for the other.

Although the single-domain superconductors are relatively nonhysteretic and thus very lightly damped, other noncontacting interactions with magnets may provide valuable damping for a flux-pinned interface. For example, a magnet near a conductive metal such as aluminum is subject to the well-known eddy-current damping effect. We performed several experiments with aluminum plates between the magnet and superconductor in the pendulum interfaces and found that the aluminum does not interfere with the flux-pinned equilibrium or stiffness, but dramatically enhances the damping of the pendulum up to strong overdamping. The results of one such damping experiment appear in Fig. 13. At the 5–6 cm separations where an aluminum plate is present, the damping ratios of each mode are enhanced. The inclusion of conductive plates to provide eddy-current damping allows flux-pinned interfaces to exhibit both high stiffness and high structural damping, which would be important to noncontacting modular spacecraft systems such as those described in Norman and Peck [2] or Gersh and Peck [3]. The properties of these conductive plates may be tailored to design FPIs with a desired damping ratio. Some configurations exhibit significant overdamping in the FFTs. This result is particularly compelling if the flux-pinned connections between modules provide the "virtual structure" of a fractionated spacecraft: Demchak recom-

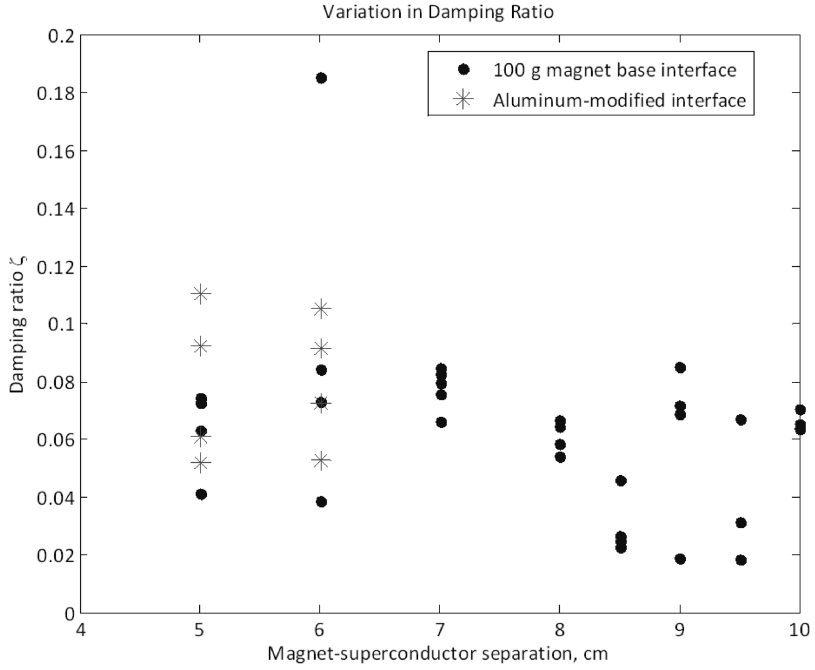

FIG. 13. Damping a Flux-Pinned Interface with a Plate of Aluminum over the Superconductor.

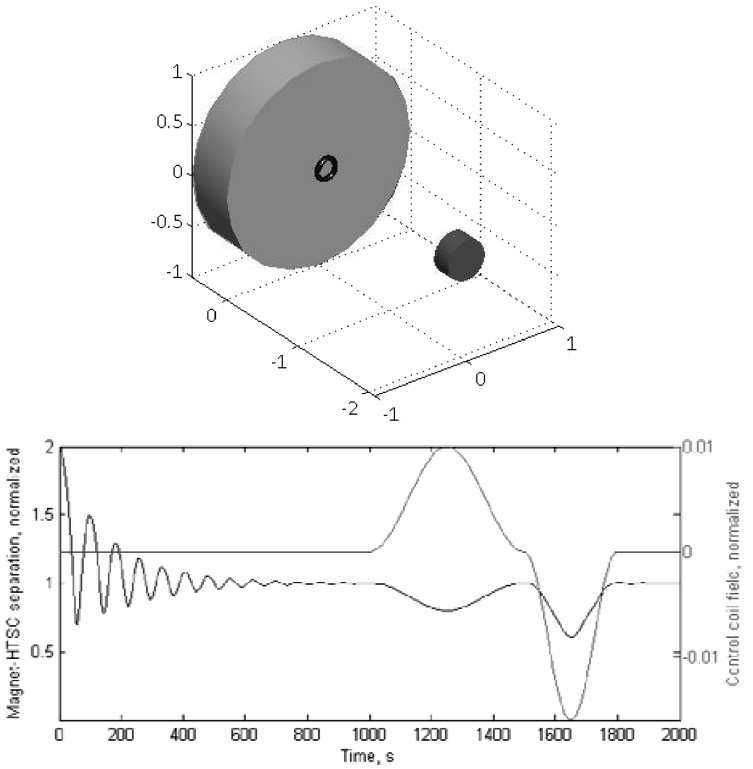

FIG. 14. *Top*: schematic of a magnet (small, dark cylinder) flux-pinned to a high-temp superconductor disc (large, light cylinder) with an electromagnet coil (dark ring) near the disc. *Bottom*: simulated time history of the magnet position and control coil field.

mends passive damping ratios be modeled at no lower than $\zeta = 0.001$ for space structures [20]. Common practice is 0.0025. A flux-pinned interface may provide an even higher level of passive damping when modules are separated by several centimeters. Therefore, a flux-pinned interface can eliminate some conservatism in dynamics analysis. They may also represent an opportunity to improve the stability margins and performance of control loops associated with these relative motions.

Along with confirming previous results, an extension of the frozen-image model suggests that nearby electromagnets can actuate a flux-pinned interface. The time history of simulated motion in a possible scenario is shown in Fig. 14. In this simulation, a magnet falls in toward a superconducting disc that has been "preloaded" with flux by field-cooling and is captured at the previously established equilibrium. The control electromagnet then activates, pulling the magnet into a new, adjustable equilibrium. Taking the z direction to be normal to the HTSC surface, this one-dimensional equilibrium is the solution of

$$0 = \frac{m^2}{(z_0 + z)^4} - \frac{m^2}{(2z)^4} + \frac{m_c m}{(z - \delta)^4} - \frac{m_c m}{(z + \delta)^4} \tag{8}$$

In this model, the permanent magnet with moment m and initial position z_0 interacts with its flux-pinning images, the control electromagnet with moment m_c and position δ, and the Meissner image of the electromagnet in the superconducting disc. An arrangement of electromagnets around a flux-pinned interface thus

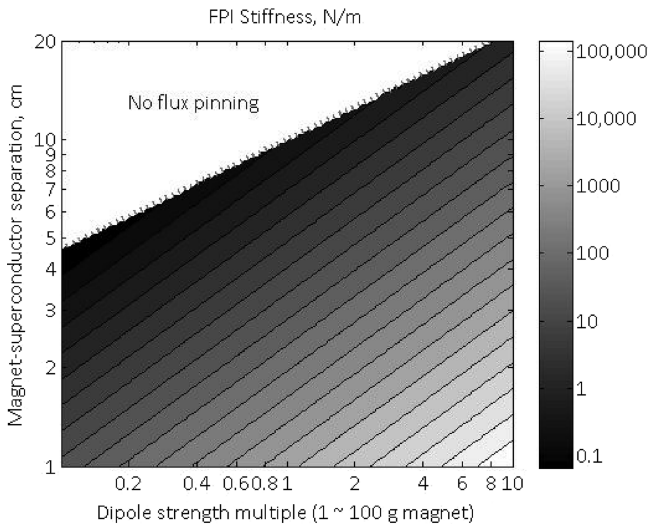

FIG. 15. Design Space of a Flux-Pinned Interface Based on the 100-g Magnet and Single-Domain YBCO in These Experiments.

offers the possibility of controlling the separation and orientation of FPI-linked components, as suggested in Fig. 3(c). Figure 1 shows an action-at-a-distance Stewart platform based on this principle. This configuration allows stable 6DOF actuation of noncontacting spacecraft modules. The dipole moment of the control electromagnet in the scenario of Fig. 14 is much smaller than that of the permanent magnet, suggesting that very little power need be applied to the actuating electromagnets. Should the actuators fail, the components remain robustly bound by the unperturbed flux-pinning stiffness provided by the permanent magnet.

Conclusion

The stiffness and damping of a flux pinning over a wide range of separations, as well as an understanding of how the interface responds to manipulations, can inform the design of flux pinning hardware for modular space systems. A design guideline of this type is shown in Fig. 15. Here, the 100 g rare-earth magnet and single-domain YBCO disc from the experiments provide the basis for simulated FPI stiffness over a range of separation distances and for a range of dipole moments. The dipole moment of a magnet corresponds roughly to the mass of the magnet, and the mass of the magnet is likely much greater than that of the YBCO; so, this result takes the magnet mass to be the significant performance parameter. The plot shows a range of achievable stiffnesses and intermodule separation distances for a modular system with flux-pinned interfaces similar to the pendulum apparatus. This magnet–superconductor configuration is not necessarily optimal in the sense that it may not project the greatest possible flux to the YBCO surface. Other configurations of magnets may be able to optimize this quantity. For example, the arrangement of permanent magnets in Fig. 16 efficiently projects magnetic flux toward a single-domain YBCO disc above it while limiting the magnetic field bias introduced to the spacecraft bus below the magnets, similar to a Halbach array [21]. These interfaces may form the basis of next-generation

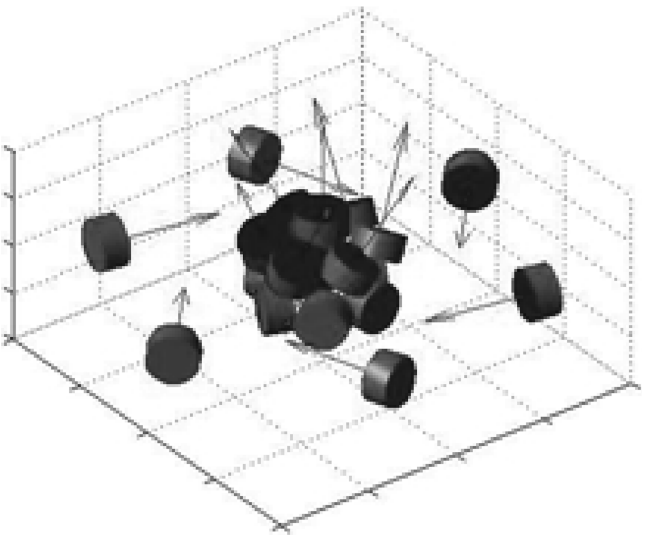

FIG. 16. Potential Arrangement of Magnets for a Flux-Pinned Interface.

docking and mating adapters or even act as a noncontacting structure supporting modular space systems with intermodule spacing on the 10 cm to 1 m scale.

The ability to alter the equilibrium separation between a flux-pinned magnet and a superconductor offers the possibility of relatively simple actuation of a flux-pinned interface. For example, introducing a perturbing field by increasing the current in a nearby electromagnet causes the equilibrium magnet–superconductor separation to change, so that spacecraft with flux-pinned interfaces would be able to adjust their relative positions, carry out docking maneuvers, and even manipulate other modules through the interfaces, without physical contact or fuel expenditure. Flux-pinning interfaces may then function as more familiar manipulators, mating adapters, and close-range formation-flight and maneuvering-hardware technologies. Such articulated systems developed on a flux-pinned "virtual structure" would be passively robust in the event of actuator failure.

The requirement that certain elements of a FPI remain below a critical temperature offers the possibility that such structures might reconfigure by toggling their flux-pinned interfaces on and off. This temperature management might be achieved simply by exposing superconductors to sunlight or shielding them from it. Interface toggling behavior is equivalent to docking and release maneuvers, but the action-at-a-distance forces involved do not require physical contact between structures at any point in the process. Reconfiguration of spacecraft modules in close proximity using flux-pinned interfaces would therefore be a low-risk activity compared to the reconfiguration of a modular system by traditional means. Toggling a flux-pinned interface in such a way would be analogous to activating and deactivating a virtual truss segment between modules.

Yet another exciting possibility relies on the feature that flux pinning does not exert forces or torques along directions of zero magnet field gradient. This feature allows the construction of modular systems where flux pinning forms the modules into a kinematic mechanism designed to facilitate reconfiguration. A noncontacting, flux-pinned mechanism architecture as in Fig. 3(b) has several advantages over both other flux-pinned reconfiguration methods and traditional close-range forma-

tion flying or docking methods. All modules may be structurally identical and contain universal interfaces. No specially constructed hinge interfaces are necessary. Activation or deactivation of electromagnets in a generic interface introduces the necessary kinematic degrees of freedom. In addition, because the modules do not come into physical contact, there is no physical wear of components, and the potential for deployable mechanisms to jam in orbit is virtually eliminated. Spacecraft reconfiguration achieved through kinematics also provides advantages and savings through a reduced reliance on active control: an appropriately selected mechanism constrains out undesirable motions kinematically, and the inherent inertia properties of the entire structure might be enough to drive the reconfiguration process without power input. At most, small internal torques (provided by, for instance, reaction wheels) may be required to rotate modules about a joint.

This investigation indicates that useful design parameters of a flux-pinned interface based on a single magnet and single superconductor include:

- The dipole moment of the magnet. Increased dipole moment gives increased stiffness at constant separation distance and increased maximum flux-pinning range.
- The hysteretic properties of the superconductor. A hysteretic superconductor provides a FPI with more inherent damping. However, hysteresis is not a desirable dynamic property of a space system, and damping can be achieved by other means.
- The amount of ferromagnetic material near the interface, particularly on the opposite side of the superconductor relative to the magnet. More ferromagnetic material changes the relative strengths of the various translational and rotational stiffnesses.
- The amount of conductive material near the interface. Conductive metals introduce eddy-current damping to the FPI.

Additional design parameters affect a flux-pinned interface. Several of those not investigated in this work are:

- The effects on stiffness and damping of other configurations of magnets and superconductors, with both elements on each face of a FPI.
- The effect of changing the amount of superconductive material present, such as using a thin-film superconductor that may provide high stiffness with some mass savings.

Further work on the flux-pinned interfaces described in this paper will allow us to begin the design process for flux-pinned, modular space systems; potentially with the ability to reconfigure their structures by forming kinematic mechanisms.

References

[1] SHOER, J. and PECK, M. "Stiffness of Flux-Pinned for Virtual Structure for Modular Spacecraft," *Journal of the British Interplanetary Society*, Vol. 62, No. 2, 2009, pp. 57–65.

[2] NORMAN, M. and PECK, M. "Stationkeeping and Reconfiguration of a Flux-Pinned Satellite Network." *Proceedings of the AIAA Guidance, Navigation, and Control Conference*, Honolulu, HI, Aug. 18–21, 72008.

[3] GERSH, J. and PECK, M. "Architecting the Very-Large-Aperture Flux-Pinned Space Telescope: A Scalable, Modular Optical Array with High Agility and Passively Stable

Orbital Dynamics." *Proceedings of the AIAA Guidance, Navigation, and Control Conference*, Honolulu, HI, Aug. 18–21, 2008.
[4] JONES, L. and PECK, M. "Prospects and Challenges of Particulate Solar Sail Propulsion." *Proceedings of the AIAA/AAS Astrodynamics Specialist Conference*, Honolulu, HI, Aug. 18–21, 2008.
[5] BRANDT, E.H. "Rigid Levitation and Suspension of High-Temperature Superconductors by Magnets," *American Journal of Physics*, Vol. 58, No. 1, 1990, pp. 43–49.
[6] DAVIS, L.C. "Lateral Restoring Force on a Magnet Levitated above a Superconductor," *Journal of Applied Physics*, Vol. 67, No. 5, 1990, pp. 2631–2636.
[7] SCHONHUBER, P. and MOON, P.C. "Levitation Forces, Stiffness, and Force-Creep in YBCO High-*Tc* Superconducting Thin Films," *Applied Superconductivity*, Vol. 2, No. 7, 1994, pp. 523–534.
[8] EARNSHAW, S. "On the Nature of the Molecular Forces which Regulate the Constitution of the Luminiferous Ether," *Transactions of the Cambridge Philosophical Society*, Vol. 7, 1842, pp. 97–112.
[9] WERNER, M. "Spitzer: The First 30 Months." *Astronomy & Geophysics*, Vol. 47, No. 6, 2006, pp. 6.11–6.16.
[10] BRANDT, E.H. "Levitation in Physics," *Science*, Vol. 243, No. 4889, 1989, pp. 349–355.
[11] SUGIURA, T., ADYAGI, T., URA, H. and YOSHIZAWA, M. "Parametrically Excited Horizontal and Rolling Motion of a Levitated Body above a High-Tc Superconductor," *IEEE Transactions on Applied Superconductivity*, Vol. 13, No. 2, 2003, pp. 2247–2250.
[12] MOON, F.C. *Superconducting Levitation*, Wiley, New York, 1994.
[13] HULL, J.R. and CANSIZ, A. "Vertical and Lateral Forces between a Permanent Magnet and a High-Temperature Superconductor," *Journal of Applied Physics*, Vol. 86, No. 11, 1999, pp. 6396–6404.
[14] JOHANSEN, T.H. *et al*. "Magnetic Levitation with High-*Tc* Superconducting Thin Films," *Journal of Superconductivity*, Vol. 11, No. 5, 1998, pp. 519–524.
[15] JOHANSEN, T.H. and BRATSBERG, H. "Theory for Lateral Stability and Magnetic Stiffness in a High-*Tc* Superconductor-Magnet Levitation System," *Journal of Applied Physics*, Vol. 74, No. 6, 1993, pp. 4060–4065.
[16] SHOER, J. and PECK, M. "Reconfigurable Spacecraft as Kinematic Mechanisms Based on Flux-Pinning Interactions." *Journal of Spacecraft and Rockets*, Vol. 46, No. 2, March–April 2009, pp. 466–469
[17] WILSON, W., SHOER, J., and PECK, M. "Demonstration of a Magnetic Locking Flux-Pinned Revolute Joint for Use on CubeSat-Standard Spacecraft." *Proceedings of the AIAA Guidance, Navigation, and Control Conference*, Chicago, IL, Aug. 10–13, 2009.
[18] KORDYUK, A. "Magnetic Levitation for Hard Superconductors," *Journal of Applied Physics*, Vol. 83, No. 1, 1998, pp. 610–612.
[19] BASINGER, S.A., HULL, J.R. and MULCAHY, T.M. "Amplitude Dependence of Magnetic Stiffness in Bulk High-Temperature Superconductors," *Applied Physics Letters*, Vol. 57, No. 27, 1990, pp. 2492–2494.
[20] DEMCHAK, L.J. "Estimating Structural Dumping" in *Spacecraft Structures and Mechanisms: From Concept to Launch*, Sarafin, T. and Larson, W. (eds). Microcosm, Inc., El Segundo, CA, 1995, p. 824.
[21] HALBACH, K. "Design of Permanent Multipole Magnets with Oriented Rare Earth Cobalt Material," *Nuclear Instruments and Methods*, Vol. 169, No. 1, 1980, pp. 1–10.